



# A rosette like carbon structure controlled through ammoniation for superior adsorption of cationic brilliant green dye

Xu Deng<sup>3</sup> · Xiaohua Feng<sup>1,2</sup> · Risheng Li<sup>4</sup> · Rongrong Li<sup>3</sup> · Ping Zhou<sup>1,2</sup> · Hua Li<sup>1,2</sup>

© The Author(s), under exclusive licence to Springer Science+Business Media, LLC, part of Springer Nature 2021

## Abstract

This paper investigates the influence of the structure, composition, pore size distribution and morphology of three carbon materials obtained from the explosion of acetylene gas on the adsorption performance of brilliant green (BG) dye. During the process, Rosette like carbon (RLC) is obtained in the detonation reaction gas with small amount of ammonia. It shows excellent adsorption properties and high reusability. The adsorption capacity is more than twice of C-nN and C-pN at the concentration of BG of 100 mg/L, the maximum monolayer adsorption capacity of 357.32 mg/g, elimination efficiency can reach 88.5% after 10 cycles of adsorbing BG, which is the best adsorption performance among the currently reported carbon materials. The adsorption equilibrium accords with Langmuir isotherm model and falls into single molecular layer absorption. The temperature and pH value selected have little effect on its adsorption capacity. The excellent properties of RLC contribute to an ideal substitute to the existing adsorbents of carbon materials.

**Keywords** Ammonia explosion · Surface structure · Porous · Brilliant green · Adsorbing performance

## 1 Introduction

In the previous research, it is found that the carbon materials with oxygen and porous structure demonstrate a good adsorption effect on dissolved lithium polysulfide [1].

However, the materials are not applicable to the treatment of toxic dyes. For example, brilliant green (BG) dye, one of the triphenylmethane dyes and commonly used in the paper, textile, plastic, rubber and fish farming industries due to its antimicrobial properties and brilliant color [2, 3]. After medical validation, excessive BG ingestion can cause coughing, shortness of breath, nausea, vomiting and diarrhea. In addition, in the water environment, the application of BG will cause carcinogenesis and gene mutation to aquatic organisms [4–7], so the removal of it from paper and dyestuff wastewater is very important for the protection of human health and ecological environment [8].

Carbon material is a good choice for adsorption of organic compounds. The performance of those adsorbents depends on its porosity, surface area and surface chemical group [9]. At present, various carbon materials are used in the adsorption of dye in aqueous, such as graphite oxide nano particles [10, 11], carbon counter electrodes [12], amorphous carbon fibers [13], carbon nanotubes [14], activated carbon derived from various biological materials [15–19], biochar prepared from plant waste [20], rice husk ash [21], porous functional carbon [22], surfactant doped Polyaniline/MWCNTs [23], Fe<sub>3</sub>O<sub>4</sub>/sawdust carbon nanocomposites [24], peat of Brunei Darussalam [25], and nitrogen doped mesoporous carbons [26], para-aminobenzoic acid modified activated

Xu Deng and Xiaohua Feng contributed equally to this work.

✉ Xiaohua Feng  
xhfeng@nimte.ac.cn

✉ Hua Li  
lihua@nimte.ac.cn

<sup>1</sup> Key Laboratory of Marine Materials and Related Technologies, Zhejiang Key Laboratory of Marine Materials and Protective Technologies, Ningbo Institute of Materials Technology and Engineering, Chinese Academy of Sciences, Ningbo 315201, China

<sup>2</sup> Zhejiang Engineering Research Center for Biomedical Materials, Cixi Institute of BioMedical Engineering, Ningbo Institute of Materials Technology and Engineering, Chinese Academy of Sciences, Cixi 315300, China

<sup>3</sup> Shaanxi University of Chinese Medicine, XiXian New Area, Xianyang 712046, China

<sup>4</sup> Institute of Land Engineering and Technology, Shaanxi Provincial Land Engineering Construction Group Co., Ltd., 710075, Xi'an, China

carbon [27], etc. Most of these carbon materials have low adsorption capacities and less cycle adsorption times [28]. Therefore, it is brought to the table to produce a new nano scale carbon material with the high specific surface area, active group, mesoporous or macro porous to improve the BG adsorption capacity and recycling rate.

The electronegativity of oxygen is stronger than that of nitrogen. For the adsorption of cationic dyes, it is expected that the doped nitrogen can enhance the affinity and adsorption for dyes. As ammoniation is a common method to change the surface and composition of materials, some reducing agent ammonia is added to the original gas acetylene and oxygen in the process of detonation, aiming to change the original morphology, structure and composition of carbon materials. Given above, a new highly porous rosette like carbon (RLC) nano-adsorbent is synthesized by industrial detonation technology using acetylene as carbon source and ammonia as reducing agent. The structure characteristics, composition, specific surface area and interaction mechanism of organic molecules BG are analyzed in detail based on kinetics balance. The results indicate that the adsorbent has excellent adsorptive capacity, desorption performance and recycling rate. To the best of our knowledge, RLC shows better removal and recycle rate than that reported in any existing literature. Moreover, RLC is used for the first time as dye absorption in aqueous solution.

## 2 Experimental

### 2.1 Fabrication of RLC materials

RLC is prepared by industrial gas explosion, the volume ratio is 10% NH<sub>3</sub>, 30% O<sub>2</sub> and 60% C<sub>2</sub>H<sub>2</sub>, they are mixed in a sealed gas tank in turn, then ignited to generate a detonation wave, carbon and carbon triple bond of the acetylene gas is opened, and recomposed to form a carbon material. C-nN is the compared sample with 40% O<sub>2</sub> and 60% C<sub>2</sub>H<sub>2</sub>. C-nN is post treated under NH<sub>3</sub> gas flow rate of 400 sccm for 4 h at 500°C with a ramp rate of 5 °C/min, the obtained black powders is named C-pN.

### 2.2 Physicochemical Characterization

SEM and TEM are respectively characterized with Hitachi S4800 (Japan) and FEI Tecnai F20 field emission scanning transmission electron microscope at 300 keV. Thermal gravimetric analysis (TGA) measurement is carried out by the heating to 800 °C at the scan rate of 5 °C/min under an atmospheric environment. The D8 Advance diffractometer X-ray diffraction (Bruker, Gemany) is adopted for the structure analysis of C with a Cu K $\alpha$  radiation. The examination of Raman spectra is carried out by the Renishaw inVia Reflex

Raman Microscope and recorded with a laser operating at 532 nm. XPS measurements are determined by an Axis Ultra DLD X-ray photoelectron spectrometer using monochromatic Al K $\alpha$  (1486.6 eV) radiation. The infrared spectrum is tested on Tensor 27 Fourier transform infrared spectrometer (German Bruker). The ASAP2020HD88 nitrogen gas sorption system is used for porosity analysis (Micromeritics instrument Corp, USA). Light absorption analysis is performed with a double beam TU-1901 UV–visible station (Beijing Puxitong Analytical Ltd., China).

### 2.3 Adsorption performance

About 4 mg RLC adsorbent add into 5 mL of BG aqueous solutions with a series of initial concentrations, then agitate on water-bath shaker (200 rpm, 25°C) for 8 h. The samples are centrifuged after incubation, and 1 mL of supernatants is taken to measure the absorbance triplicated under identical conditions at 623 nm [29], this is the maximum absorption peak of BG. Then calculate the average value. The adsorption capacity of BG per unit mass of adsorbent adopt the following formula (1).

$$q_e = \frac{(c_0 - c_e)V}{W} = \frac{(A_0 - A_e)V_{C_0}}{WA_0} \quad (1)$$

$q_e$  (mg/g) is the amount of adsorbent adsorbed at equilibrium,  $c_0$  (mg/L) is the initial concentration of adsorbate,  $c_e$  (mg/L) is the concentration of adsorbate at equilibrium,  $V$  (mL) is the volume of adsorbate solution,  $W$  (mg) is the mass of adsorbent,  $A_0$  is the initial absorbance of dye solution without adsorbent, and  $A_e$  is the equilibrium absorbance with adsorbent.

The remove efficiency ( $R_E$ , %) is calculated by the following formula at equilibrium (2).

$$R_E = \frac{(c_0 - c_e)}{c_0} \times 100\% = \frac{(A_0 - A_e)}{A_0} \times 100\% \quad (2)$$

Four isotherm models (Langmuir, Freundlich, Temkin, Langmuir–Freundlich and Redlich–Paterson) are applied to fit the adsorption equilibrium respectively, the models equations [19] are listed in the Table S1.

## 3 Results and discussions

### 3.1 Carbon material analysis

In the SEM and TEM images, the morphology of C- nN and C-pN is formed by winding the bent ribbon graphene (Fig. 1b, c, e, f) with similar structure and particle size of about 50 nm (Fig. 1a, d). This indicates that the

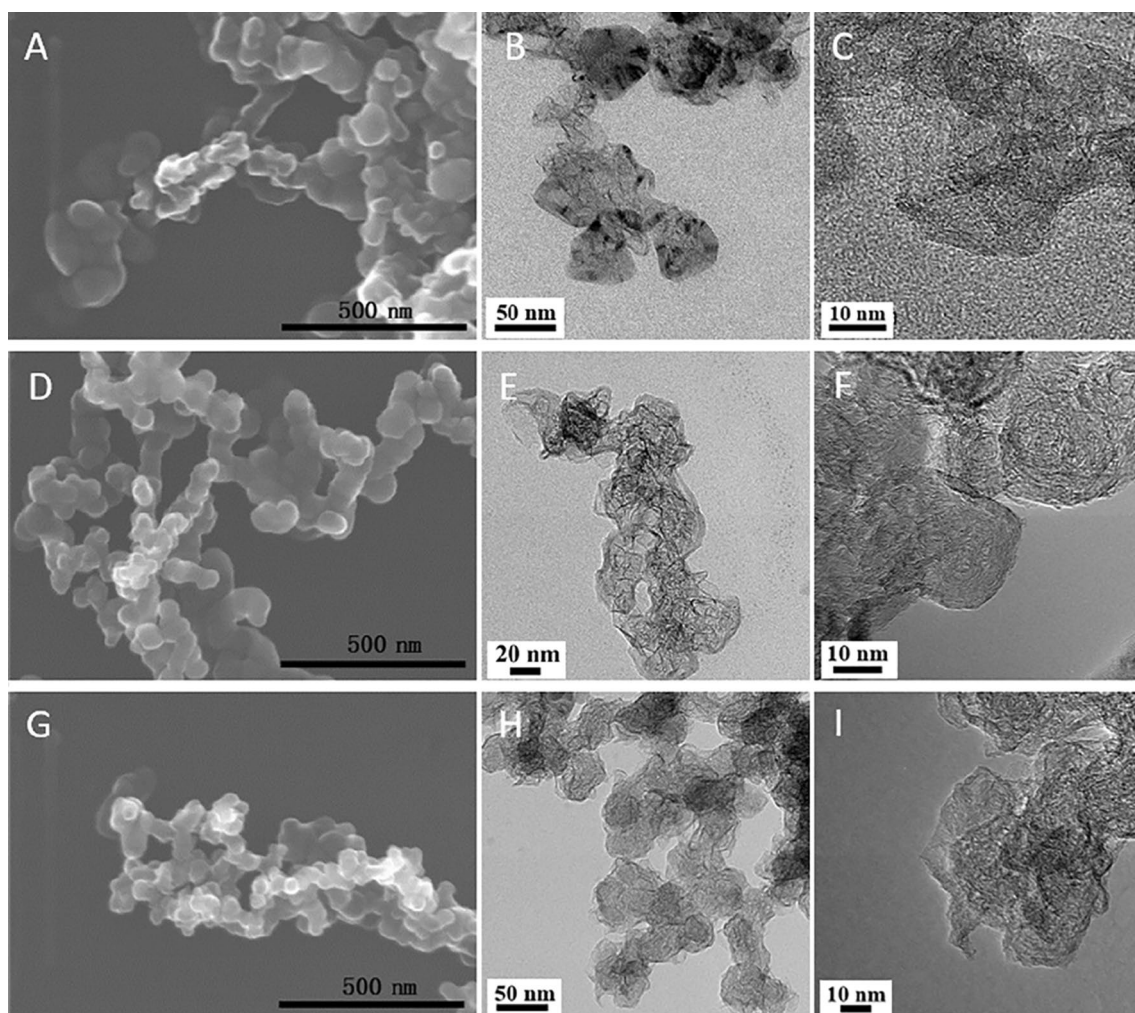


**Fig. 1** SEM images (a, d, g) of C-nN, C-pN, RLC respectively; TEM images (BC, EF, HI) of C-nN, C-pN, RLC respectively

post-treatment of ammonia has little effect on the morphology of materials. While the size of RLC is slightly smaller, about 40 nm, and the particles are more evenly distributed (Fig. 1g). The addition of ammonia as the original reaction gas changes the morphology of the material, showing rose-flower-like structure, which means more curved lamellar structure exposed with multilayer graphene about 5–15 layers (Fig. 1h, i). This structure seems to have more contact sites with organic macromolecules, which can improve the dye adsorption capacity.

It can be seen from the TGA test (Fig. 2a), the thermal stability of C-nN is very good at room temperature and until 700 °C, and the weight loss begins to increase due to oxidation once the temperature rises higher than 700 °C. RLC materials start to oxidize slowly at 500°C, while C-pN start to oxidize at 300 °C and above. When the temperature rises to 800 degrees Celsius, the remaining amount of C-nN, C-pN and RLC materials is 70.8%, 35.5% and 36.3% respectively (Table 1).

The carbon XRD curves (Fig. 2b) of C-nN and C-pN materials contain graphene oxide peak at 19°, indicating post treatment of ammonia cannot reduce the graphene oxide of C-nN material. In general, the peak of graphite appears at about 26° corresponding to its (002) plane. The curves of C-pN has the strongest graphite peak with the highest degree of graphitization, which is consistent with the result of the Raman test. Obviously, RLC peak at this position shifts to the left, showing a wider peak, which may correspond to the amorphous peak of carbon. It means that ammonia, as the primary detonation gas, participates in the reaction and promotes an amorphous carbon structure being formed. Normally, the peak corresponding to the (111) face of diamond is at 44°, both RLC and C-pN contain weak peaks at this position, indicating that the ammonia gas tends to induce the crystal form from  $sp^2$  to  $sp^3$  hybrid, especially as an original reactive gas. We speculate that some  $sp^3$  hybrid carbon atoms may be in the flower center of RLC, and carbon atom connection forms at the beginning of detonation process.

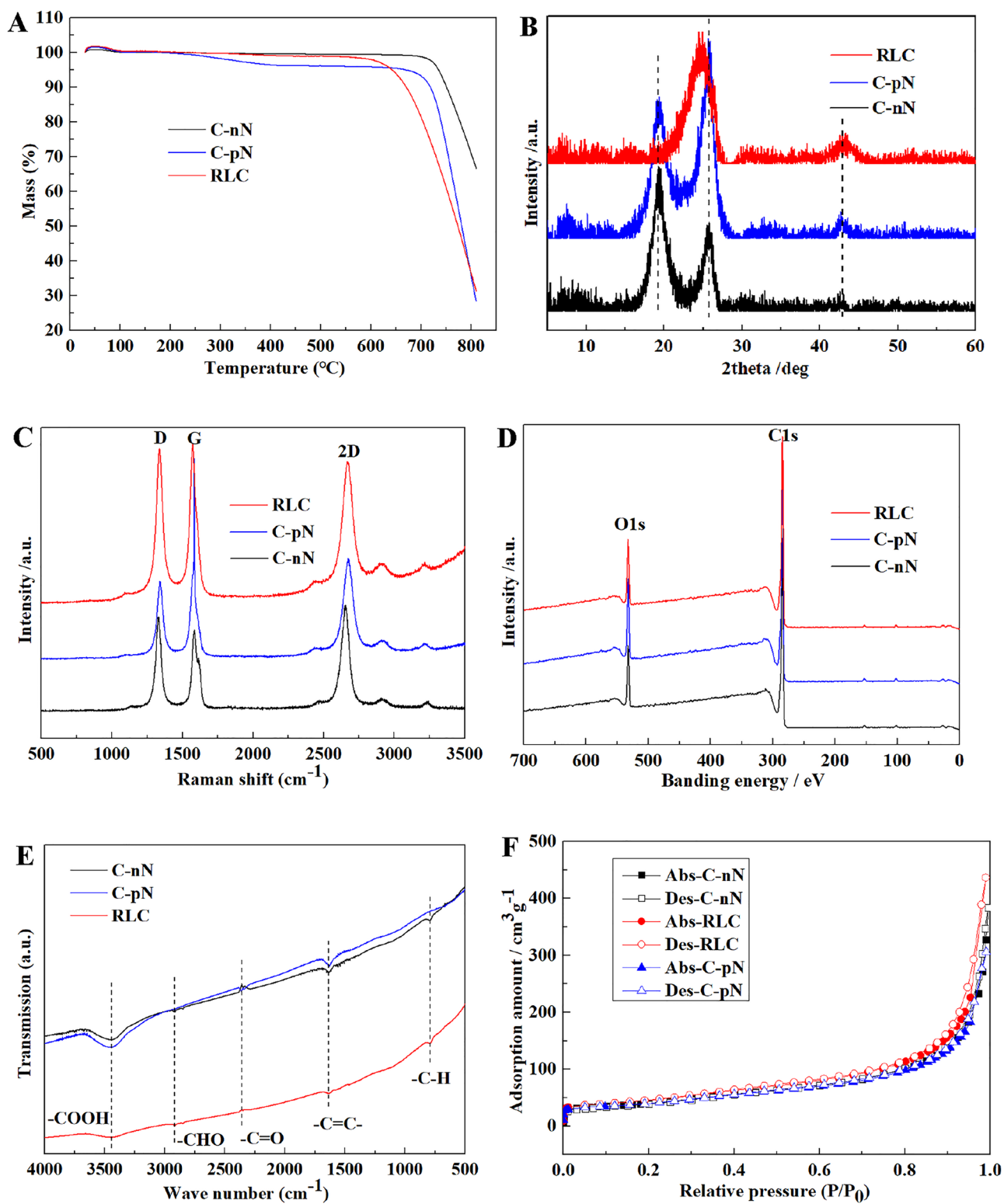


**Fig. 2** TGA curves (a), XRD curves (b), Raman spectra (c), XPS spectra (d), FTIR spectrum (e) and BET spectrum (f) of the three carbon materials

**Table 1** Summary the thermal stability results of the three carbon materials

Temperature (°C)	C-nN	C-pN	RLC
	Mass (%)		
30.0	100.1	100.3	100.4
100.0	100.1	100.2	100.5
200.0	100.0	99.8	100.1
300.0	99.8	98.2	99.8
400.0	99.6	96.4	99.2
500.0	99.5	96.2	99.0
600.0	99.4	95.9	98.0
650.0	99.3	95.5	93.9
700.0	98.8	93.2	81.3
750.0	90.2	73.0	61.0
800.0	70.8	35.5	36.3

Subsequent, the bent graphene structure with  $sp^2$  hybrid is formed.

The Raman spectrum of carbon nanomaterials usually has three main characteristics: D peak, G peak, and 2D peak (Fig. 2c). The D peak at around  $1335\text{ cm}^{-1}$  is attributed to the structural disorder and defects near the edge of the microcrystalline structure, indicating the lattice defects inside. The G peak at around  $1580\text{ cm}^{-1}$  represents the  $sp^2$  vibration mode of the graphene plane, this is a sign of the crystallinity of the carbon material, and this means that the three carbon materials contain a certain amount of nanocrystalline. Generally, the ratio of G/D is used to represent the degree of graphitization of carbon materials. The values of G/D are 0.87, 2.52, 1.03 for C-nN, C-pN, RLC, respectively. It shows that C-pN has the highest degree of graphitization after ammonia post-treatment, and the layer structure of graphite is relatively complete. The 2D peak at  $2665\text{ cm}^{-1}$  is related to the number of graphene layers. On the right side of the 2D peak, the spectrum of RLC has a tendency of upwarping, indicating that this material has a certain absorption in the near-infrared region and may have a certain fluorescence effect.

It can be observed from the XPS pattern that all three carbon materials contain oxygen atoms on the surface (Fig. 2d). At about 400 eV, the N atom 1s orbital peak is not obvious (near 400 eV) and exceeds the error range of XPS test. Perhaps the amount of nitrogen atoms introduced is too small.

The infrared spectrum curves of the three carbon materials show that they all contain the absorption peak of C–O (Fig. 2e), while the peak intensity of RLC is the weakest. The absorption peak near  $3500\text{ cm}^{-1}$  cannot be confirmed whether it is the absorption peak of the O–H of the carboxyl group or the absorption peak of the N–H. It shows that the ammonia gas, as a reaction gas, has a strong chemical reduction effect.

Through the  $N_2$  adsorption desorption figures (Fig. 2f), the amount of  $N_2$  adsorbed by RLC is slightly higher than that of the other two carbon materials. It shows that ammonia gas as a reaction gas can increase the specific surface area. The specific surface area of C-nN, C-pN and RLC are 141.8, 158.4, and  $164.5\text{ m}^2/\text{g}$ , respectively. Large specific surface area can adsorb more BG molecules to improve the adsorption capacity of carbon materials.

### 3.2 Adsorption properties

The adsorption capacity of the three materials on BG is tested (Figure S1). RLC adsorption capacity is more than twice of C-nN and C-pN at the concentration of BG of 100 mg/L, showing the porous amorphous carbon materials have better adsorption properties for BG. Hence we focus on the study of the adsorption properties of RLC hereinafter.

The pH value of solution affects the RLC surface charge and ionization degree of BG, which additionally affects the adsorption property [30]. When pH value ranges from 3 to 11, the adsorption capacity and removal efficiency are almost unaffected (Fig. 3a). It means the competition between the protonation of BG,  $H_3O^+$  and  $OH^-$  with adsorbate cations for adsorption active sites is not obvious, which results in little change in the large pH value range.

The initial BG concentration and contact time in the adsorption process are evaluated over, three BG solutions of different concentrations and at different time intervals. The adsorption capacity increases drastically in the beginning stage (Fig. 3b), demonstrating the availability of readily accessible sites on RLC surface. Higher initial BG concentration, higher  $q_t$  value is obtained, because the high concentration offers significant drive force to conquer the transfer resistance between RLC and solution mass. Besides, it is obviously observed that the equilibrium time at different initial concentrations is basically the same (Fig. 3b), that means the time required for BG molecules to reach the surface adsorption site of RLC is consistent. Furthermore, we investigate the adsorption capacity of seven different concentrations in 30 min of adsorption (Fig. 3c), the amount of 300 mg/L basically can reach the saturated adsorption concentration with the largest quantity. Generally, high temperature is beneficial for heat and mass transfer, and ultimately affects the amount of molecules adsorbed. However, the temperature is not sensitive to this adsorption process (Fig. 3d), that means the temperature has little effect on the number of adsorbent active sites. It is an advantage in various applications.

The interaction between BG and RLC is described by adsorption isotherm. Six isotherm models (i.e. linear and non-linear Langmuir, Freundlich, Temkin, Langmuir–Freundlich and Redlich–Peterson) are applied to investigate the equilibrium property (Table S1). Through comparison, the

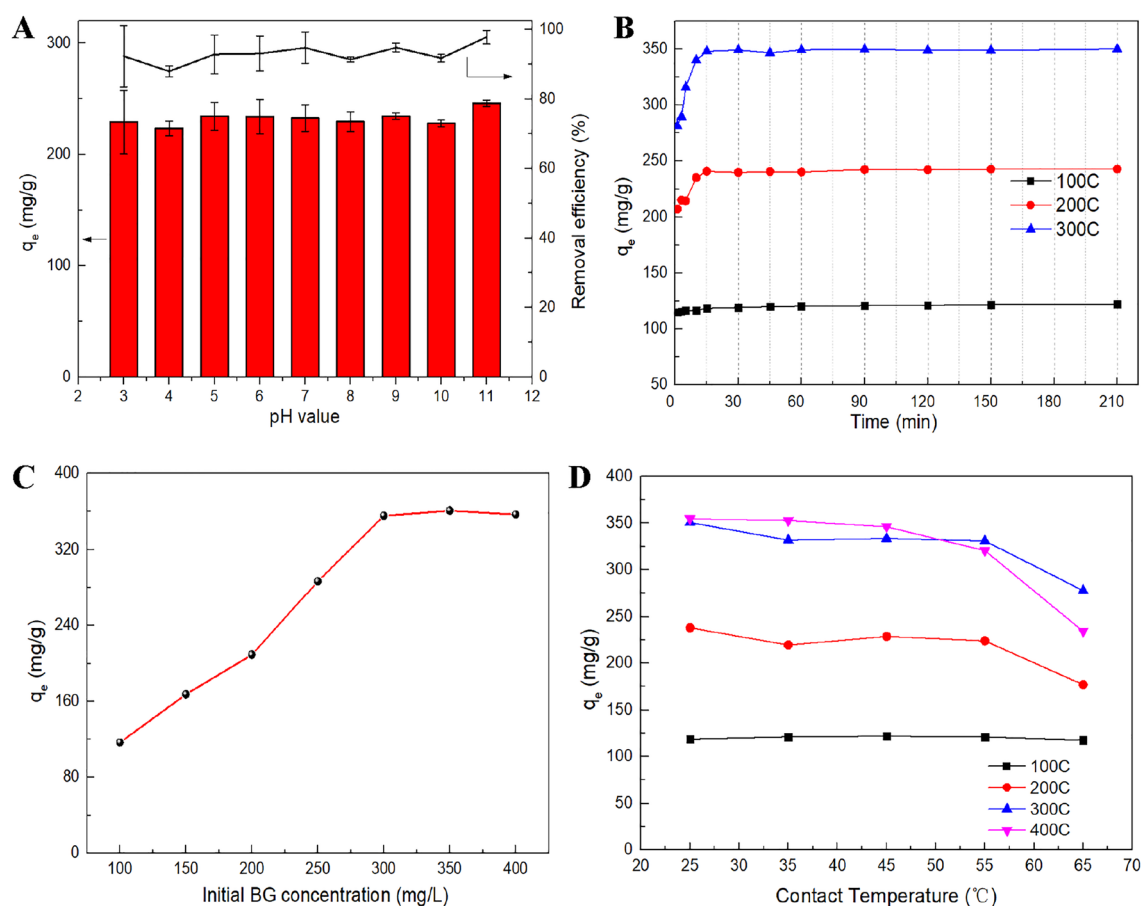


**Fig. 3** Effect of (a) initial solution pH, (b) contact time, (c) initial concentration and (d) contact temperature on adsorption capacity

correlation coefficient of Freundlich model is less satisfactory ( $R^2=0.693$ , linear;  $R^2=0.760$ , non-linear) (Table S2 and Figure S2), which is not well matched with the experimental data and fails to explain these isotherm data. The value of the Redlich-Paterson constant ( $g=1.018$ ) is almost close to 1, that means the adsorption process is more inclined to Langmuir isothermal model (Figure S3). Generally speaking, the Freundlich isotherm model assumes that the adsorption process is multi-layer adsorption. Obviously, this model is not suitable for this adsorption process. The Langmuir parameter is used to predict the affinity between BG and RLC, which is illustrated by the dimensionless separation factor ( $R_L$ ), given by the following equation [31]:

$$R_L = \frac{1}{1 + bC_0} \quad (3)$$

$R_L$ : dimensionless separation factor;  $C_0$ : initial adsorbate concentration (mg/L);  $b$ : Langmuir constant (L/mg).  $R_L$  is normally described the difficulty of the adsorption process. It is not conducive to adsorption when  $R_L > 1$ , it

is linear adsorption when  $R_L = 1$ , it is good for adsorption when  $0 < R_L < 1$ , or it is reversible adsorption when  $R_L = 0$ . In the concentration range of 100–600 mg/L, the  $R_L$  value is between  $1.01 \times 10^{-1}$  and  $1.84 \times 10^{-2}$  (Figure S4), indicating the system is a favorable adsorption process, which has a higher affinity between BG and RLC. As the initial concentration of BG increases, the value of  $R_L$  gradually decreases, indicating high initial concentration is beneficial to the adsorption process. The maximum monolayer adsorption capacity of 357.32 mg/g, which is much higher than that other carbon materials mentioned in the current literatures (Table 2). The high adsorption capacity of RLC can be attributed to high specific surface area and amorphous structure. Ammonia as the original gas can effectively improve the crystal structure, specific surface area and carbon skeleton accumulation form of carbon materials using detonation process, furtherly improving the adsorption capacity on BG dye. It is also worth mentioning that the changed surface and structure of as-made carbon materials are attained through high-volume manufacturing technology.

**Table 2** Comparison of the maximum adsorption of BG onto various carbon adsorbents

Adsorbents	Maximum adsorption capacity (mg/g)	References
Rice husk ash	25.13	[32]
Bagasse fly ash	133.33	[29]
Ashoka leaf powder	125	[33]
Oxidized cactus fruit peel	142.85	[34]
Rice straw biochar	111.11	[20]
Activated carbon from acorn	2.11	[35]
Kaolin	65.42	[36]
NaOH treated saw dust	58.48	[37]
MPN	79.8	[38]
Red Clay	125	[39]
Activated carbon	20.83	[16]
Bottom ash	28.92	[40]
Graphite oxide	124.74	[10]
EDTA modified Fe <sub>3</sub> O <sub>4</sub> /sawdust carbon	285.7	[24]
RLC	<b>357.32</b>	Our work

### 3.3 Recycling performance

Desorption studies are used to further explain the mechanism of adsorption and restore the adsorbent. The methanol solution is a suitable desorbent for desorbing the BG dye on RLC (Figure S5), and desorption rate can reach more than 95%. The polar solubility of methanol is very well in organic solvents, the hydroxyl group of methanol forms hydrogen bond with water to increase solubility. This means that hydrogen bond interaction is the main control mechanism during the desorption process. There should be a weak van der Waals force or a weak hydrogen bond between BG and RLC. Renewability studies show that RLC can reach 88.5% elimination efficiency after 10 cycles of adsorbing BG, this is the best recycling performance for BG reported in the literature.

Fourier-transform infrared spectra of RLC and BG dye-loaded RLC are obtained between 4000 and 500 cm<sup>-1</sup> (Figure S6). The broad band at 3346 cm<sup>-1</sup> of uncontaminated RLC relates to O–H groups, 1636 cm<sup>-1</sup> assigns to the skeletal vibration of aromatic C=C bonds and the small bands between 1100 and 1500 cm<sup>-1</sup> ascribe to COO<sup>-</sup> anion stretching. It can be found that some new peaks appear with others disappear in the FTIR spectrum of RLC after BG adsorption. The bands at 2950–2990 cm<sup>-1</sup> are related to the stretching vibrations of C–H bonds. Loaded BG on RLC is demonstrated by the loss of characteristic O–H groups. Some absorption peaks showing in the range of 1000–1800 cm<sup>-1</sup> are caused by the adsorption of dyes on RLC.

## 4 Conclusion

Our work researched the RLC fabricated from acetylene gas detonation method with 10% NH<sub>3</sub> as reducing agent. The material was then used to remove BG dye in aqueous. RLC had a nearly amorphous rose like structure and oxygenated functional group, which improved the BG adsorption capacity tremendously. The adsorption capacity of RLC is twice than that of C-nN and C-pN. The maximum monolayer adsorption capacity of RLC is 357.32 mg/g, which is much better than that of the carbon materials reported at present. Moreover, the adsorption of BG by RLC is not sensitive to the aqueous pH and temperature, which can be used in various conditions. After elution by methanol eluent, the adsorption performance of RLC remains excellent, which can be recycled for more than 10 times. As the original reaction gas, ammonia can improve the crystal structure and morphology of carbon materials, and additionally the adsorption performance for BG. Simple ammonia post-treatment process cannot achieve such effect. The structure and composition of carbon materials can be further modified through optimizing the detonation parameters.

**Supplementary Information** The online version contains supplementary material available at <https://doi.org/10.1007/s10934-021-01067-3>.

**Acknowledgements** This work was supported by the National Natural Science Foundation of China through Grant no. 51802322, the S&T Innovation 2025 Major Special Programme of Ningbo (2018B10054), K. C. Wong Education Foundation (Grant # GJTD-2019-13), Chinese Academy of Sciences Key Project (ZDRW-CN-2019-3) and the Natural Science Foundation of Shaanxi Province no. 2020JQ-857.

## References

1. X. Feng et al., New structural carbons via industrial gas explosion for hybrid cathodes in Li–S batteries. *Sustain. Chem. Eng.* **7**, 12948–12954 (2019)
2. H. Tavallali, M. Ostovar, Trace spectrophotometric determination of brilliant green in fish farming water samples. *Int. J. Chemtech Res.* **1**, 199–203 (2009)
3. D. Ziolkowska et al., Adsorption of cationic and anionic dyes onto commercial kaolin. *Adsorpt. Sci. Technol.* **27**(2), 205–214 (2009)
4. S. Seshadri, P.L. Bishop, A.M. Agha, Anaerobic/aerobic treatment of selected azo dyes in wastewater. *Waste Manag.* **14**, 127–137 (1994)
5. G. McKay, M. Otterburn, J. Aga, Fuller's earth and fired clay as adsorbents for dye-stuffs. *Water Air Soil Pollut.* **24**, 307–322 (1985)
6. A.R. Gregory, J. Elliott, P. Kluge, Ames testing of direct black 38 parallels carcinogenicity testing. *J. Appl. Toxicol.* **1**, 308–313 (1981)
7. K.G. Bhattacharyya, A. Sarma, Adsorption characteristics of the dye, brilliant green, on neem leaf powder. *Dyes Pigments* **57**, 211–222 (2003)
8. M.G. Mohamed et al., Multifunctional hypercrosslinked porous organic polymers based on tetraphenylethene and triphenylamine

- derivatives for high-performance dye adsorption and supercapacitor. *Polymers* **12**(10), 2426 (2020). ((1–17))
9. K.I. Aly et al., A facile synthetic route and dual function of network luminescent porous polyester and copolyester containing porphyrin moiety for metal ions sensor and dyes adsorption. *Microporous Mesoporous Mater.* **298**, 110063 (2020). ((1–11))
  10. N. Zeinali, M. Ghaedi, G. Shafie, Competitive adsorption of methylene blue and brilliant green onto graphite oxide nano particle following: derivative spectrophotometric and principal component-artificial neural network model methods for their simultaneous determination. *J. Ind. Eng. Chem.* **20**(5), 3550–3558 (2014)
  11. A. Molla et al., Selective adsorption of organic dyes on graphene oxide: theoretical and experimental analysis. *Appl. Surf. Sci.* **464**, 170–177 (2019)
  12. M. Wu et al., Carbon counter electrodes in dye-sensitized and perovskite solar cells. *Adv. Funct. Mater.* **30**(7), 1906451 (2020). ((1–34))
  13. R.R.I. Neto, R.J.S.M. Raj, The flash effect in electronic conductors: the case of amorphous carbon fibers. *Scripta Mater.* **179**, 20–24 (2020)
  14. W. Zhang, S.R.P. Silva, Reversible functionalization of multi-walled carbon nanotubes with organic dyes. *Scripta Mater.* **63**(6), 645–648 (2010)
  15. M. Vasuki, S. Punitha, M. Karthika, A comparative study of adsorption of acid blue 9 and brilliant green from aqueous solution by activated carbon derived from coconut shell and palmyra fruit nut shell. *J. Adv. Appl. Sci. Res.* **1**(7), 1–5 (2017)
  16. V. Rawat et al., *Oplismenus frumentaceus* (Jhangora) husk for activated carbon preparation and its use in adsorption of Brilliant Green dye from aqueous solution. *J. Indian Chem. Soc.* **90**(8), 1223–1231 (2013)
  17. A. Jaiswal, M.C. Chattopadhyaya, Studies of kinetics and isotherm effect on Brilliant Green dye with activated carbon. *J. Indian Chem. Soc.* **86**(12), 1315–1319 (2009)
  18. M. Ghaedi et al., Solid phase extraction and removal of brilliant green dye on zinc oxide nanoparticles loaded on activated carbon: new kinetic model and thermodynamic evaluation. *J. Ind. Eng. Chem.* **20**(4), 1444–1452 (2014)
  19. M. Asadullah et al., Chemical and structural evaluation of activated carbon prepared from jute sticks for Brilliant Green dye removal from aqueous solution. *J. Hazard. Mater.* **174**(1–3), 437–443 (2010)
  20. M.S. Ur Rehman et al., Adsorption of brilliant green dye on biochar prepared from lignocellulosic bioethanol plant waste. *Clean: Soil, Air, Water* **44**(1), 55–62 (2016)
  21. M.P. Tavlieva et al., Kinetic study of brilliant green adsorption from aqueous solution onto white rice husk ash. *J. Colloid Interface Sci.* **409**, 112–122 (2013)
  22. R.L. Liu et al., Biomass-derived highly porous functional carbon fabricated by using a free-standing template for efficient removal of methylene blue. *Biores. Technol.* **154**, 138–147 (2014)
  23. R. Kumar, M.O. Ansari, M.A. Barakat, Adsorption of brilliant green by surfactant doped polyaniline/MWCNTs composite: evaluation of the kinetic, thermodynamic, and isotherm. *Ind. Eng. Chem. Res.* **53**(17), 7167–7175 (2014)
  24. N. Kataria, V.K. Garg, Application of EDTA modified Fe<sub>3</sub>O<sub>4</sub>/sawdust carbon nanocomposites to ameliorate methylene blue and brilliant green dye laden water. *Environ. Res.* **172**, 43–54 (2019)
  25. H.I. Chieng, N. Priyantha, L.B.L. Lim, Effective adsorption of toxic brilliant green from aqueous solution using peat of Brunei Darussalam: isotherms, thermodynamics, kinetics and regeneration studies. *RSC Adv.* **5**(44), 34603–34615 (2015)
  26. H.C. Chen et al., Nitrogen doping effects on the physical and chemical properties of mesoporous carbons. *J. Phys. Chem. C* **117**(16), 8318–8328 (2013)
  27. M. Naushad et al., Adsorption of textile dye using para-aminobenzoic acid modified activated carbon: Kinetic and equilibrium studies. *J. Mol. Liq.* **296**, 112075 (2019). ((1–7))
  28. I. Anastopoulos et al., Removal of caffeine, nicotine and amoxicillin from (waste)waters by various adsorbents. A review. *J. Environ. Manag.* **261**, 110236 (2020). ((1–9))
  29. V.S. Mane, I.D. Mall, V.C. Srivastava, Use of bagasse fly ash as an adsorbent for the removal of brilliant green dye from aqueous solution. *Dyes Pigments* **73**(3), 269–278 (2007)
  30. J.T. Li et al., A wormhole-structured mesoporous carbon with superior adsorption for dyes. *Carbon* **49**(6), 1912–1918 (2011)
  31. K.R. Hall et al., Pore- and solid-diffusion kinetics in fixed-bed adsorption under constant-pattern conditions. *Ind. Eng. Chem. Fundam.* **5**(2), 212–223 (1966)
  32. V.S. Mane, I.D. Mall, V.C. Srivastava, Kinetic and equilibrium isotherm studies for the adsorptive removal of Brilliant Green dye from aqueous solution by rice husk ash. *J. Environ. Manag.* **84**(4), 390–400 (2007)
  33. G. Neha, K.K. Atul, M.C. Chattopadhyaya, Adsorption studies of cationic dyes onto Ashoka (*Saraca asoca*) leaf powder. *J. Taiwan Inst. Chem. Eng.* **43**(4), 604–613 (2012)
  34. R. Kumar, M.A. Barakat, Decolourization of hazardous brilliant green from aqueous solution using binary oxidized cactus fruit peel. *Chem. Eng. J.* **226**, 377–383 (2013)
  35. M. Ghaedi et al., A novel acorn based adsorbent for the removal of brilliant green. *Desalination* **281**(17), 226–233 (2011)
  36. B.K. Nandi, A. Goswami, M.K. Purkait, Adsorption characteristics of brilliant green dye on kaolin. *J. Hazard. Mater.* **161**(1), 387–395 (2009)
  37. V.S. Mane, P.V.V. Babu, Studies on the adsorption of Brilliant Green dye from aqueous solution onto low-cost NaOH treated saw dust. *Desalination* **273**(2–3), 321–329 (2011)
  38. M. Bagtash, J. Zolgharnein, Removal of brilliant green and malachite green from aqueous solution by a viable magnetic polymeric nanocomposite: Simultaneous spectrophotometric determination of 2 dyes by PLS using original and first derivative spectra. *J. Chemom.* **32**(7), 1–9 (2018)
  39. M.S.U. Rehman et al., Adsorption of Brilliant Green dye from aqueous solution onto red clay. *Chem. Eng. J.* **228**, 54–62 (2013)
  40. A. Mittal, D. Kaur, J. Mittal, Applicability of waste materials-bottom ash and deoiled soya-as adsorbents for the removal and recovery of a hazardous dye, brilliant green. *J. Colloid Interface Sci.* **326**(1), 8–17 (2008)

**Publisher's Note** Springer Nature remains neutral with regard to jurisdictional claims in published maps and institutional affiliations.